Journal of Materials Chemistry C

PAPER

Cite this: J. Mater. Chem. C, 2015, 3, 4632

Controllable assembly of multicarboxylic acids functionalized heteropolyoxomolybdates and allochroic properties†

Yanfen Liang,[a] Suzhi Li,[b] Donghui Yang,[a] Pengtao Ma,[a] Jingyang Niu*[a] and Jingping Wang*[a]

Received 30th January 2015,
Accepted 25th March 2015

DOI: 10.1039/c5tc00297d

www.rsc.org/MaterialsC

A series of inorganic–organic hybrid heteropolyoxomolybdates built from $[TeMo_6O_{21}]^{2-}$ polyoxoanions and multicarboxylic acids including $(C_3N_2H_5)_4H_6[(TeMo_6O_{21})_2\{O_2C(CH_2)_2CO_2\}_3]\cdot 9.5H_2O$ (**1**), $(C_3N_2H_5)_8H_2[(TeMo_6O_{21})_2\{O_2C(CH_2)_6CO_2\}_3]\cdot 3.5H_2O$ (**2**) and $(CN_3H_4)_{16}H_4[(TeMo_6O_{21})_4\{C_6H_3(COO)_3\}_4]\cdot 16H_2O$ (**3**) have been synthesized arising from the reactions of $(NH_4)_6Mo_7O_{24}\cdot 4H_2O$, Na_2TeO_3/TeO_2 and the corresponding multicarboxylic acids in an aqueous medium. X-ray single crystal diffraction, X-ray powder diffraction (XPRD), elemental analyses, inductively coupled plasma (ICP) spectra, IR spectra, UV spectra and thermogravimetric (TG) analyses have been implemented. Crystal structure analyses reveal that both compounds **1** and **2** are dimers, while **3** is a tetramer, however, they contain the same $\{TeMo_6\}$ unit which consists of a six-membered MoO_6 octahedral ring capped by one $\{TeO_3\}$ trigonal pyramid. Compounds **1–3** exhibit intriguing allochroic properties. They can change color from white to blue/green when heated. Upon the irradiation of a xenon lamp (full wave-band, P = 300 W), their color can change from white to reddish brown.

Introduction

Over the years, interest in inorganic–organic hybrid compounds based on polyoxometalates (POMs) has greatly expanded because they have diverse structures and many applications in various areas ranging from catalysis, medicine, electrochemistry, photochromism, to magnetism and materials science.[1] Among the hybrids, functionalized POMs with organic ligands have a dominant position. A variety of approaches have been taken advantage of, in order to incorporate organic moieties in polyoxoanions, and derivatization results in the stabilization of otherwise unstable molecular architectures, as well as providing novel building blocks for the assembly of larger systems.[2]

Carboxylic acids are a type of oxygen-containing ligand, that not only have rich structures, but can also easily coordinate to metallic atoms by taking over the oxo group of POMs. Compared to monocarboxylic acids, multicarboxylic acids are often adopted to synthesize larger and more diverse hybrids, because they have more oxygen coordination atoms to connect two or more polyoxoanions. Polyoxomolybdates (PODs), act as a kind of inorganic POM cluster, and play an important role in constructing inorganic–organic POM hybrids. Moreover, many hybrids based on PODs and organic cations (mainly organoammonium) have intriguing allochroic properties, which can be applied as materials for smart windows, cosmetics, multicolor smart painting, UV sensors, optical power-limiting switches, three-dimensional (3D) high-density optical data storage, chill checkers, cooking tools, hotplates, furnaces and so on.[3,4] As a subset of organic ligand functionalized POMs, hybrids based on carboxylic acids and PODs have been researched, uninterruptedly.[5–12] Up to date, many carboxylic acid functionalized POD anions have been reported, such as $\{MoO_2\}^{2+}$,[6a] $\{(MoO_2)_4\}^{8+}$,[6b] $\{(MoO_2)_8\}^{8+}$,[6a] $\{Mo_2O_4\}^{2+}$,[6c] $\{Mo_4O_8\}^{4+}$,[6d] $\{Mo_6O_{13}\}^{8+}$,[7] $\{Mo_{10}O_{30}\}^{4-}$,[8a] $\{Mo_{10}O_{32}\}^{4-}$,[8b] $\{Mo_{18}O_{52}(OH)_4\}^{8-}$,[9] $\{(\mu_3\text{-}OH)_4Mo^{V}_{20}Mo^{VI}_{34}O_{164}\}^{28-}$,[10] $\{(OH)_{10}Mo^{V}_{20}Mo^{VI}_{26}O_{134}\}^{22-}$,[10] $\{Mo_{2n}O_{2n}S_{2n}(OH)_{2n}\}$,[5,11] $\{HPMo_6O_{21}\}^{2-}$,[12a] $\{SeMo_6O_{21}\}^{2-}$,[12b] $\{AsMo_6O_{21}\}^{3-}$ (ref. 12c) and so on. Moreover, most of them have interesting structures and attractive properties such as photochromism and electrocatalysis influenced by the ligands.[11f,13] In these derivatives, hetero-PODs are less reported compared with iso-PODs. In addition, for the carboxylic acid functionalized $\{XMo_6\}$ (X = P, Se, As) units, the dimension and composition can be stereochemically oriented and conformationally ordered by different

[a] Key Laboratory of Polyoxometalate Chemistry of Henan Province, Institute of Molecular and Crystal Engineering, College of Chemistry and Chemical Engineering, Henan University, Kaifeng 475004, Henan, China. E-mail: jpwang@henu.edu.cn, jyniu@henu.edu.cn; Fax: +86 37123886876

[b] College of Chemistry and Chemical Engineering, Engineering Research Center of Functional Material Preparation, Shangqiu Normal University, Shangqiu, 476000, Henan, China

† Electronic supplementary information (ESI) available: X-ray crystallographic details (CIF), UV spectra, Tables S1–S3, and Fig. S1–S15. CCDC 1027004, 1027005 and 1028993. For ESI and crystallographic data in CIF or other electronic format see DOI: 10.1039/c5tc00297d

carboxylic acids,[12] so a target assembly by ligand control can be provided.

Telluromolybdates have been studied for a long time as a member of the hetero-PODs, in which most of them are derivatives based on an Anderson-type cluster $[TeMo_6O_{24}]^{6-}$, where the Te atom is hexavalent. Comparatively, hetero-PODs containing Te^{IV} atom are rare, whereas, Te^{IV} is known to exhibit a variety of coordination modes, such as $\{TeO_3\}$ trigonal pyramids, $\{TeO_4\}$ with SF_4 geometry, and $\{TeO_5\}$ square pyramids.[14] Tetravalent tellurium is, therefore, more interesting from the structural point of view. Despite Kortz and co-workers having reported a series of amino acid functionalized telluromolybdates,[2] carboxylic acid functionalized telluromolybdates have never been reported. Like the derivatives based on $[HPMo_6O_{21}]^{2-}$, $[SeMo_6O_{21}]^{2-}$ and $[AsMo_6O_{21}]^{3-}$ clusters,[12] carboxylic acid functionalized telluromolybdates may also be targeted by using different carboxylic acid ligands. Thus, in this context, hetero-PODs containing a Te^{IV} atom are taken advantage of to react with succinic acid, suberic acid and 1,3,5-benzenetricarboxylic acid ($btcH_3$) separately and two dimers $(C_3N_2H_5)_4H_6[(TeMo_6O_{21})_2\{O_2C(CH_2)_2CO_2\}_3]\cdot 9.5H_2O$ (**1**), $(C_3N_2H_5)_8H_2[(TeMo_6O_{21})_2\{O_2C(CH_2)_6CO_2\}_3]\cdot 3.5H_2O$ (**2**) and a tetramer $(CN_3H_4)_{16}H_4[(TeMo_6O_{21})_4\{C_6H_3(COO)_3\}_4]\cdot 16H_2O$ (**3**) are successfully obtained. As expected, the structures of these hybrids are controlled by the different ligands. Furthermore, heating and irradiation were carried out for compounds **1–3** and they present interesting thermosensitive and photochromic properties.

Experimental

Materials

All the chemical reagents were used as purchased, without further purification.

Synthesis

$(C_3N_2H_5)_4H_6[(TeMo_6O_{21})_2\{O_2C(CH_2)_2CO_2\}_3]\cdot 9.5H_2O$ (1). The synthesis of **1** was accomplished by dissolving 0.530 g (0.429 mmol) of $(NH_4)_6Mo_7O_{24}\cdot 4H_2O$ in 20 mL of water with stirring, then adding 0.111 g (0.500 mmol) of Na_2TeO_3, 0.354 g (3.000 mmol) of succinic acid, 0.087 g (0.500 mmol) of caesium chloride, and 0.085 g (1.250 mmol) of imidazole with stirring, to get a cloudy white solution, whose pH was 4.5. The solution was refluxed with stirring for an hour and then cooled to room temperature. The pH of the resultant clear colorless solution was still 4.5. The solution was filtered into a 50 mL beaker. Slow evaporation of the filtrate at room temperature led to block colorless crystals of **1** suitable for X-ray diffraction, after two weeks. Yield: 45.6% (0.328 g) for **1** based on $(NH_4)_6Mo_7O_{24}\cdot 4H_2O$. Anal. calcd (%) for **1**: Mo 39.97, Te 8.86, C 10.01, H 1.99, N 3.89; Found: Mo 40.29, Te 8.98, C 10.12, H 2.18, N 3.98. IR (KBr pellet): 3450 (s), 3144 (s), 2842 (m), 2627 (m), 1625 (w), 1552 (s), 1417 (s), 1231 (m), 1184 (w), 1096 (m), 1052 (m), 930 (s), 903 (s), 756 (s), 646 (s), 495 (s), 411 cm^{-1} (m).

$(C_3N_2H_5)_8H_2[(TeMo_6O_{21})_2\{O_2C(CH_2)_6CO_2\}_3]\cdot 3.5H_2O$ (2). The synthesis of **2** was accomplished by dissolving 0.132 g (0.107 mmol) of $(NH_4)_6Mo_7O_{24}\cdot 4H_2O$ in 5 mL of water with stirring, then adding 0.020 g (0.125 mmol) of TeO_2, 0.033 g (0.188 mmol) of suberic acid, 0.014 g (0.125 mmol) of tetramethylammonium chloride (TMA), and 0.021 g (0.313 mmol) of imidazole. The mixture was stirred for half an hour and a muddy white solution, whose pH was 5.3, was obtained. Then, the solution was sealed in a 25 mL stainless steel autoclave with a Teflon liner and kept at 130 °C for 72 hours. After cooling to room temperature slowly, the solution was filtered into a 25 mL beaker. Slow evaporation of the filtrate at room temperature led to block colorless crystals of **2** suitable for X-ray diffraction the next day. Yield: 18.9% (0.038 g) for **2** based on $(NH_4)_6Mo_7O_{24}\cdot 4H_2O$. Anal. calcd (%) for **2**: Mo 35.83, Te 7.94, C 17.94, H 2.67, N 6.98. Found: Mo 36.20, Te 8.10, C 18.12, H 2.78, N 7.13. IR (KBr pellet): 3442 (s), 3142 (s), 2960 (m), 2853 (m), 1625 (w), 1552 (s), 1429 (s), 1295 (w), 1173 (w), 1095 (m), 1050 (m), 930 (s), 903 (s), 748 (s), 644 (s), 499 (s), 423 cm^{-1} (m).

$(CN_3H_4)_{16}H_4[(TeMo_6O_{21})_4\{C_6H_3(COO)_3\}_4]\cdot 16H_2O$ (3). The synthesis of **3** was accomplished by dissolving 0.530 g (0.429 mmol) of $(NH_4)_6Mo_7O_{24}\cdot 4H_2O$ in 20 mL of water with stirring, then adding 0.111 g (0.500 mmol) of Na_2TeO_3, 0.105 g (0.500 mmol) of 1,3,5-benzenetricarboxylic acid, and 0.119 g (1.250 mmol) of guanidine hydrochloride with stirring to obtain a cloudy white solution, whose pH was 5.1. The solution was refluxed with stirring for an hour and cooled to room temperature. The pH of the resultant clear colorless solution was 5.3. Then, the solution was filtered into a 50 mL beaker. Slow evaporation of the filtrate at room temperature led to block colorless crystals of **3** suitable for X-ray diffraction the next day. Yield: 8.5% (0.066 g) for **3** based on $(NH_4)_6Mo_7O_{24}\cdot 4H_2O$. Anal. calcd (%) for **3**: Mo 37.10, Te 8.22, C 10.06, H 1.82, N 10.83. Found: Mo 37.55, Te 8.43, C 10.01, H 2.01, N 10.68. IR (KBr pellet): 3415 (s), 3357 (s), 3176 (s), 1661 (s), 1602 (w), 1547 (s), 1440 (s), 1373 (s), 1102 (w), 937 (s), 892 (s), 772 (w), 724 (s), 652 (s), 524 (m), 425 cm^{-1} (w).

Physical measurements

IR spectra were recorded on a Bruker VERTEX 70 IR spectrometer using KBr pellets in the range 4000–400 cm^{-1}. C, H and N elemental analyses were performed on a PerkinElmer 2400-II CHNS/O analyzer. ICP spectra (Te and Mo) were obtained on a PerkinElmer Optima 2100 DV ICP-OES spectrometer. XPRD analysis data were recorded on a Bruker D8 Advance instrument with Cu Kα radiation (λ = 1.5418 Å) in the angular range 2θ = 5–45° at 293 K. UV spectra were determined on a HITACHI U-4100 UV-Vis-NIR spectrometer (distilled water as solvent) in the range of 400–200 nm. The electron paramagnetic resonance (EPR) experiment was performed on a Bruker ER-2000-DSRC10 spectrometer at the X-band at 300 K. Diffuse reflectivity spectra were collected at room temperature on a finely ground sample with a Cary 5000 spectrometer (Varian) equipped with a 60 mm diameter integrating sphere. Diffuse reflectivity was measured from 350 to 800 nm (*i.e.*, from 3.54 to 1.55 eV) with a 2 nm step using non-absorbing $BaSO_4$ powder as a reference. The samples were irradiated with a PLS-SXE 300 type xenon lamp. Thermogravimetric analyses were measured on a Mettler-Toledo

TGA/SDTA 851[e] analyzer under a nitrogen gas atmosphere, with a heating rate of 10 °C min^{-1} from 25 °C to 800 °C.

X-ray single crystal diffraction

The single crystals of compounds **1–3** were encapsulated in a glass tube for indexing and intensity data collection at 296 K on a Bruker APEX-II CCD diffractometer using graphite-monochromated Mo Kα radiation (λ = 0.71073 Å). Routine Lorentz and polarization corrections were applied, and an absorption correction was performed using the SADABS program. Direct methods were used to solve the structure and refined by full-matrix least-squares on F^2 using the SHELXTL-97 program package. Non-hydrogen atoms were refined anisotropically. Moreover, NH_4^+ and lattice H_2O could not be distinguished based on electron densities, and we thus determined the lattice water molecules and NH_4^+ ions by elemental analysis. The crystallographic and experimental details of the crystal structure determinations are given in Table 1. The CCDC reference numbers 1027004, 1027005, 1028993 are for compounds **1–3**, respectively.

Results and discussion

Syntheses

The covalent grafting of organic components onto POM clusters makes POMs have more diverse structures and more applications. Carboxylic acids, as a subclass of organic groups, have aroused extensive interest because of their multiple structures and their characteristic easy coordination. Carboxylic acid functionalized hetero-PODs have been researched by our group and several series of derivatives based on $[HPMo_6O_{21}]^{2-}$, $[SeMo_6O_{21}]^{2-}$ and $[AsMo_6O_{21}]^{3-}$ polyoxoanions have been obtained, where the polymerization degrees of the compounds were dependent on the carboxylic acid ligands.[12] Actually, these simple chemical systems made planning the rational design and synthesis of covalently functionalized POMs become possible, because the formation of these POM species could be drastically altered by different carboxylic acids. The compounds were dimers when the ligands were aliphatic acids, with two carboxyl groups at the different sides of the zigzag carbon chain, but larger polymers, rather than analogues formed when they were at the same sides of the carbon chain.[12b] When aromatic carboxylic acids were taken advantage of as organic ligands, more novel structures controlled by the ligands would form. For example, a hexameric compound formed when pyridine-2,6-dicarboxylic acids were coordinated to the $\{SeMo_6\}$ units,[12b] while a cage tetramer formed when we used 1,3,5-benzenetricarboxylic acid with three carboxyl groups on the same plane as the ligand to coordinate to the $\{AsMo_6\}$ units.[12c] Parallel experiments revealed that suitable crystals for single crystal X-ray diffraction (XRD) could be obtained in lower yields, without caesium chloride existing in the reaction solution for compound **1**. Meanwhile, when the amount of succinic acid was reduced four times, **1** could not be obtained. These results indicated that the ionic strength of the solution influenced by CsCl affected the yield of compound **1** and the proportion of the reagents was important for the formation of **1**. Compound **2** could not be formed if TMA was not added to the solution, which might be due to TMA influencing the ionic strength of the reaction solution. Interestingly, **2** could be obained if we refluxed the reaction solution for an hour, but the resultant crystal was not suitable for single crystal XRD, which indicated that the crystal morphology of **2** was affected by the reaction temperature and pressure. In the synthesis of compound **3**, the

Table 1 Crystallographic data for compounds **1–3**

	1	**2**	**3**
Formula	$C_{24}H_{57}Mo_{12}N_8O_{63.5}Te_2$	$C_{48}H_{85}Mo_{12}N_{16}O_{57.5}Te_2$	$C_{52}H_{112}Mo_{24}N_{48}O_{124}Te_4$
M_r (g mol^{-1})	2880.21	3212.74	6206.65
Space group	*R*32	*P*2(1)/*c*	*Pnma*
Cryst. syst.	Hexagonal	Monoclinic	Orthorhombic
a (Å)	20.8647(11)	18.325(3)	28.781(3)
b (Å)	20.8647(11)	12.758(2)	28.635(2)
c (Å)	16.3866(10)	21.500(3)	25.140(2)
α (deg)	90	90	90
β (deg)	90	90.822(3)	90
γ (deg)	120	90	90
V (Å^3)	6177.9(6)	5026.2(13)	20 719(3)
Z	3	2	4
Cryst. size (mm^3)	0.50 × 0.32 × 0.23	0.25 × 0.21 × 0.17	0.50 × 0.28 × 0.25
D_{calcd} (g cm^{-3})	2.398	2.104	1.959
μ (mm^{-1})	1.062	2.111	2.048
R_{int}	0.0782	0.0364	0.0442
Limiting indices	$-24 \le h \le 24$	$-18 \le h \le 21$	$-34 \le h \le 34$
	$-24 \le k \le 23$	$-15 \le k \le 12$	$-19 \le k \le 34$
	$-19 \le l \le 11$	$-25 \le l \le 24$	$-29 \le l \le 29$
No. of reflns collected	10 669	25 293	103 427
No. of independent reflns	2463	8817	18 571
No. of params	155	475	1015
GOF on F^2	1.062	1.054	1.081
R_1, wR_2 [$I > 2\sigma(I)$]	0.0483 0.1332	0.0497 0.1344	0.0532 0.1534
R_1, wR_2 [all data]	0.0505 0.1359	0.0688 0.1443	0.0813 0.1712

addition of guanidine hydrochloride promoted the formation of suitable crystals of **3**. It was not feasible when we used the same method as compound **2** to synthesize **1** and **3**. The research we had conducted indicated that the carboxylic acid ligands influenced the synthetic methods of **1–3**. Crystals of **1–3** were easily converted to powders on exposure to air, due to weathering. Compared with the series of compounds based on $[HPMo_6O_{21}]^{2-}$, $[SeMo_6O_{21}]^{2-}$ and $[AsMo_6O_{21}]^{3-}$ polyoxoanions, the formation of derivatives based on the $[TeMo_6O_{21}]^{2-}$ polyoxoanion needed more severe reaction conditions, demonstrating that the syntheses might be related to the properties of the central atoms of the polyoxoanions.

Structures of the polyoxoanions

X-ray crystal structure analyses revealed that compounds **1–3** all contain the {$TeMo_6$} unit (Fig. 1a), which consists of a central heteroatom Te surrounded by a ring of six MoO_6 octahedra sharing edges and corners alternately, and the center Te atom is located slightly above the plane formed by the six Mo atoms and coordinates to three μ_3-oxo groups to obtain a trigonal pyramid. Each carboxyl group of the carboxylate ligands is bonded with two edge-sharing Mo centers on the same side of the ring.

In polyoxoanions of **1** and **2**, two {$TeMo_6$} units are linked by three succinic acid or suberic acid linkers (Fig. 1b and c). Both {$TeMo_6$} units are arranged in a face-to-face mode, appearing nearly superimposed. As tetradentate ligands, three dicarboxylic acids act as pillars within the formed scaffold structures. Because of the screwed torsion, two {$TeMo_6$} planes are slightly staggered due to the flexibility of the succinic acids and suberic acids with quite closed angles (about 0.6° for **1** and 2.7° for **2**).

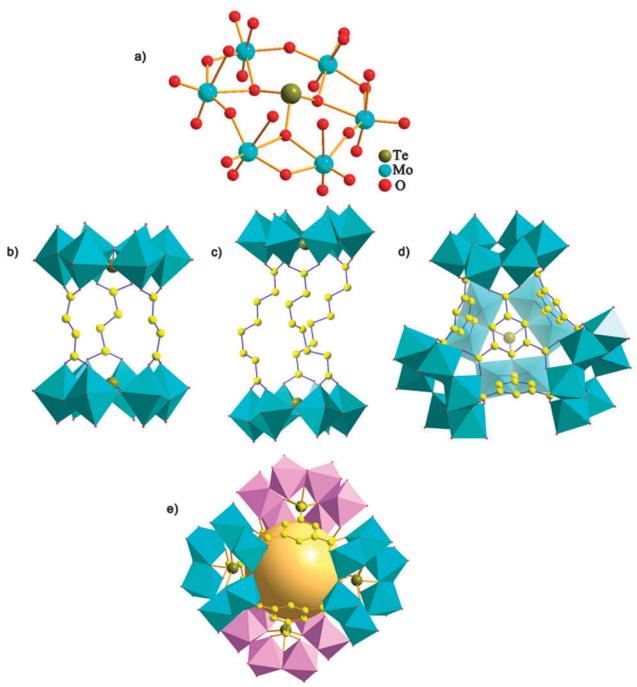

Fig. 1 Ball-and-stick/polyhedral representation of {$TeMo_6$} (a), compound **1** (b), compound **2** (c), compound **3** (d) and structure of the molecular cage in **3** (e) (MoO_6 octahedra, turquoise/pink; C atom, yellow; Te atom, dark yellow), and hydrogen atoms are omitted for clarity.

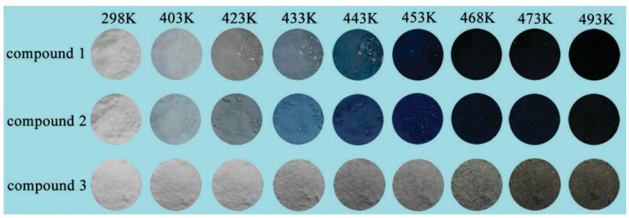

Fig. 2 Color of compounds **1–3** at different temperatures.

The polyoxoanion of compound **3** is a cage, as expected. In the polyoxoanion, btc are hexadentate ligands. The {$TeMo_6$} units and the btc act as the three-connected units that four btc covalently coordinate to four {$TeMo_6$} units, through carboxyl groups, as represented in Fig. 1d. As a result, a large hole, which has an inner cavity diameter of approximately 7.8 Å and large inner volume of about 248.5 $Å^3$ framed by the 24 carbon atoms of the four btc ligands formed (Fig. 1e).

Thermosensitivity of compounds 1–3

Investigations into X-chromic (X = photo, thermo, electro, *etc.*) materials, *i.e.*, compounds that undergo a well-observed color change upon the application of an external stimulus, have been extensive over the past decade.[16] Compounds **1–3** presented striking allochroic characteristics when they were heated, or irradiated, at ambient conditions.

Powders of compounds **1–3** were heated sequentially at 313 K, 353 K, 393–493 K in the interval of 5 K in air with each temperature sustained for an hour to research their thermosensitivity. As represented in Fig. 2, the three hybrids began to change color when the powder samples were heated to 403 K, and the color of compounds **1–2** became blue-mazarine, while compound **3** became green-celadon with the increase in temperature. In addition, the color of **1–3** started to become black, because of carbonization, when the temperature reached 468 K, and the degree of carbonization deepened as the temperature increased. Comparatively, the powder of $(NH_4)_6Mo_7O_{24}{\cdot}4H_2O$ did no exhibit a thermosensitive behavior when heated (see Fig. S2 in the ESI†). After leaving the color-changed samples at ambient conditions, or at a low temperature (6 °C) for days, their color did not change.

In order to explore the thermosensitive mechanism, UV spectra and UV-vis diffuse reflectance spectroscopy were obtained for **1–3**. From 298 to 493 K, the peak locations of the UV spectra had almost no change, indicating the preservation of the {$TeMo_6$} unit during the heating process (see Fig. S3 in the ESI†). As for the solid UV-vis diffuse reflectance spectroscopy (see Fig. S4 in the ESI†), an absorption band in the visible region arose for compounds **1–3**, with the increase in temperature, which was attributed to the intervalence charge transfer ($Mo^{5+} \rightarrow Mo^{6+}$) bands of heteropoly anions and was characteristic of heteropoly blues,[17] thus demonstrating the existence of pentavalent Mo atoms in the color-changed samples. The presence of Mo^{5+} could also be proved by EPR spectra. The compounds **1–3** exhibited no significant EPR signals at room temperature before heating. However, after heating, the color-changed powders of **1–3** showed significant paramagnetic

signals which were attributed to Mo^{5+} with g = 1.934 for **1**, 1.930 for **2** and 1.928 for **3** (see Fig. S5 in the ESI†).[12a,18] In addition, bond valence sum parameters (BVS) calculations for compounds **1–3** revealed that all of the Mo atoms were hexavalent in their ground state (see Table S1 in the ESI†). Thus, during the heating process, Mo^{6+} was reduced to Mo^{5+}.

Furthermore, we obtained variable temperature (VT) IR spectra and VT XPRD for compounds **1–3** by using their powder samples under ambient conditions (see Fig. S6 and S7 in the ESI†) to explore the structure changes of the compounds during the thermosensitive process. For compounds **1–2**, the VT IR spectra were similar. The skeleton vibrations between 4000–400 cm^{-1} were maintained from 298 to 433 K. Additionally, when the temperature was higher than 450 K, the peaks appeared to have obvious changes. Meanwhile, for compound **3**, the peaks in the range 4000–400 cm^{-1} were maintained from 298 to 453 K. In the VT XPRD of compounds **1** and **2**, the peaks showed little change before 440 K, and for compound **3**, the main peaks of its XPRD spectrum changed until 473 K, which was accordance with the variations of the VT IR spectra. Moreover, the results of the VT IR spectroscopy and the VT XPRD were close to the results of the thermogravimetric analyses.

According to the results of the series research, the proposed mechanism of the thermosensitive process could be described as heating triggering the hexavalent Mo atoms being reduced to pentavalent Mo atoms. As the temperature rose, more and more Mo^{VI} was reduced to Mo^{V}, and the color became deeper and deeper. When the temperature rose to a certain value, the structures of the compounds were destroyed, but the {$TeMo_6$} units were maintained when the temperature was as high as 493 K.

Photochromism of compounds 1–3

Powder samples of compounds **1–3** were irradiated by a xenon lamp under ambient conditions to investigate the photochromic properties and as expected, they displayed interesting color changes. The powder samples of **1–3** all showed a white color in the ground state, and became reddish brown after irradiation. However, their color change behaviors were different. As shown in Fig. 3, the speed of the color change for compound **1** was obviously slower than for **2** and **3**. After turning off the lamp, the color slowly faded by putting the colored samples in the dark for more than a dozen days under ambient conditions. When the colored samples were left at a low temperature (6 °C) or under natural light irradiation, the speed of fading was not obviously accelerated. Diffuse reflectance spectra with different irradiation time in the 350–800 nm range for compounds **1–3** were performed and the reflectivity values transformed by the Kubelka–Munk function were calculated. As represented in Fig. S8 in the ESI,† a strong absorption band peak at 447 nm for **1**, 458 nm for **2** and 466 nm for **3** showed and gained in intensity, which was associated with the irradiation time. UV spectroscopy proved the maintenance of the {$TeMo_6$} units during the photochromic process depending on the unchanging peak locations in the region 200–400 nm (see Fig. S9 in the ESI†). XPRD analysis was performed, and all of the peak positions had little variation after irradiation, which revealed no obvious structural changes during the photochromic process (see Fig. S10 in the ESI†). The EPR spectra of the color-changed samples are shown in Fig. S11 in the ESI.† The reddish brown samples of **1–3** showed paramagnetic signals with g = 1.929, g = 1.931 and g = 1.932 separately, which were attributed to the signals of Mo^{V}, indicating the existence of Mo^{V} atoms in the color-changed samples. When compounds **1–3** were irradiated by sunlight for more than a dozen hours, no color change occurred. In addition, when powder of $(NH_4)_6Mo_7O_{24}{\cdot}4H_2O$ was irradiated under a xenon lamp, no color variation occurred in the sample (see Fig. S12 in the ESI†).

During this study, all of the powder samples of the compounds **1–3** turned to reddish brown in the end, and such a coloration had been observed in other solid samples of PODs, indicating the formation of $Mo^{V}O_5(OH)$.[16,19,20] We can explain the photochromic mechanism in terms of Yamase's model. That is to say, the xenon lamp excitation transfers an electron from a terminal oxygen atom of the POM block to the adjacent Mo^{6+} ($4d^0$) site. Subsequently, this is followed by a proton transfer along the N–H···O hydrogen bond from the N to a bridged O atom at the photoreduced site and simultaneously the resulting N atom interacts with the hole left on the terminal O to form a charge–transfer complex (Scheme 1).[12a,20] During this process, the N–H···O hydrogen bond derives from the interaction of the protonated imidazole or guanidine hydrochloride and the POD blocks (see Table S2 in the ESI†).

Fig. 3 Color of compounds **1–3** after certain minutes irradiation by a xenon lamp.

Analyses of different coloration behaviors of compounds 1–3

In order to explain the different behaviors of compounds **1–3** during the allochroic processes, we superficially analysed the kinetics of the coloration process.

For the thermosensitivity, because the loss of lattice water and the rupture of hydrogen bonds require energy, so the different behaviors of compounds **1–3** during the thermosensitive process can be explained by the different numbers of the lattice water molecules, as well as the N–H···O hydrogen bonds

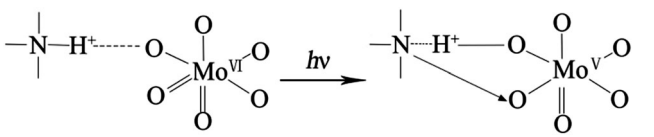

Scheme 1 The mechanism for the photochromism of compounds **1–3**.

and the optical band gap in the ground state. As shown in Fig. 4, the optical gap of the three compounds in their ground state is **3** > **1** > **2**, and the number of lattice water molecules is **3** > **1** > **2**, and the number of hydrogen bonds is **3** > **2** > **1** (see Table S2 in the ESI†), so at any temperature the hue intensity of compound **3** is weaker than **1** and **2**.

As for the photochromism, kinetic equations for compounds **1–3** were obtained according to the diffuse reflectance spectra, which are based on the theory developed by Dessapt's group.[3a] Fig. 5 shows the reflectivity values at the maximum wavelength of the absorption ($R^{\lambda max}$) *versus* the irradiation time (t) in the range 350–800 nm for compounds **1–3**. The $R^{\lambda max}$ values decrease sharply at first and then tend to flatten under irradiation, which is due to the decrease of concentration of the photoreducible Mo^{VI}, on the basis of a pseudo-second-order kinetic law. It was found that the curves of $R^{\lambda max}(t)$ *vs.* t for compounds **1–3** can be fitted by the function $R^{\lambda max}(t) = a/(bt + 1) + R^{\lambda max}(\infty)$, and the relative parameters related to the coloration kinetics of the compounds **1–3** are listed in the inset in the figure. The coloration speed is signified by $t_{1/2}$ (coloration kinetic half-life time), and the values are calculated as 27.78 min for **1**, 9.90 min for **2** and 5.15 min for **3**. That is, the coloration speed is **3** > **2** > **1**, being consistent with the coloration behaviors of compounds **1–3**. As the optical band gap is **3** > **1** > **2** (Fig. 4) and the number of hydrogen bonds is **3** > **2** > **1** (see Table S2 in the ESI†), so it is proposed that both the optical band gap and the hydrogen bonds affect the coloration behaviors during the photochromism.

As for the different colors of compounds **1–3** under xenon lamp irradiation (from white to reddish brown) and by heating (from white to blue/green), the reasons may be as follows: (1) the difference in the allochroic mechanism. For photochromic behaviors of compounds **1–3**, the mechanism is on the basis of Yamase's model, while for the thermosensitive properties, the process of the electron transfer in the hetero-PODs is not clear. Also, the different means of electron transfer may lead to different coloration behaviors. (2) The energies triggering the allochroic behaviors under irradiation and by heating are different, which may be one reason to explain the different colors. (3) During the heating process, the lattice water is gradually lost, while under xenon lamp irradiation, the water

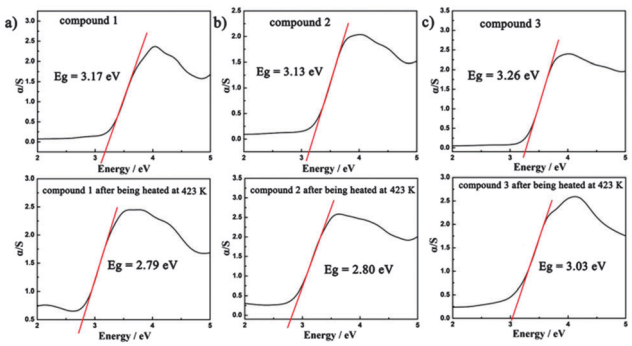

Fig. 4 UV-vis diffuse reflectance spectra of K–M functions *vs.* energy (eV) of compounds **1–3** before and after being heated at 423 K.

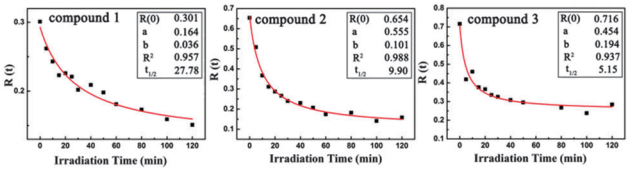

Fig. 5 Reflectivity $R(t)$ *vs.* t plots for **1** measured at 447 nm, **2** at 458 nm and **3** at 466 nm for 0, 5, 10, 15, 20, 25, 30, 40, 50, 60, 80, 100 and 120 min irradiation by xenon lamp.

is maintained, for the most part. Under irradiation, the hybrid inorganic–organic materials based on PODs and organo-ammonium cations show various color changes, such as from white to pink, brown, purple, blue and reddish brown and so on, indicating the color changes are affected by the structures and compositions of the hybrids.[3,8b,12a,16,21] Compared to photochromism, the thermosensitivity of such hybrids are less covered and most of the color changes are from white to blue.[12] So, the different coloration behaviors of compounds **1–3** under irradiation and from heating are influenced by many factors, and the definite explanations cannot be presented for the lack of theory.

X-ray powder diffraction analyses

The XPRD patterns for compounds **1–3** are exhibited in Fig. S13 in the ESI.† The diffraction peaks of both the simulated and experimental patterns match closely in key positions, thus indicating the phase purities of compounds **1–3**. The differences in the intensity between the experimental and simulated XPRD patterns may be due to the variation in the preferred orientation of the powder samples during the collection of the experimental XPRD.

FT-IR spectra

IR spectra were used to investigate the structural characters of compounds **1–3** (see Fig. S14 in the ESI†). The spectra show similar characteristic peaks for the skeletal vibrations in the region between 400 and 1000 cm^{-1}, indicating that compounds **1–3** almost have the same basic framework, which is in good agreement with the results of the X-ray single crystal structural analysis. The characteristic peaks of strong absorption bands in the range 937–892 cm^{-1} are assigned to the vibration bands of the terminal Mo=O units, and the ones in the range 772–644 cm^{-1} are assigned to the vibrations of the Mo–O–Mo groups, leading to an overlap with the ν(Te–O) stretching vibration bands.[15a] The carboxylic characteristic vibration bands (1661–1373 cm^{-1}) of compounds **1–3** all shift to low frequency in comparison with uncoordinated acid (1721–1404 cm^{-1}) as a result of the carboxyl groups interaction with metal ions.[15b] The strong bands at 3450–3415 cm^{-1} are probably because of the presence of lattice water molecules, and the signals appearing at 3176–3142 cm^{-1} are attributed to the ν(NH) stretching vibrations. In addition, the bands at 2842 cm^{-1} for **1** and 2853 cm^{-1} for **2** are assigned to the $\nu(CH_2)$ stretching vibrations. The assignment of the characteristic bands of compounds **1–3** is given in Table S3, in the ESI.†

Thermogravimetric analyses

The thermal decomposition processes of compounds **1–3** between 25–800 °C are shown in Fig. S15 in the ESI.† For compound **1**, the first weight loss of 6.04% (calc. 5.94%) between 25–163 °C corresponds to the release of 9.5 lattice water molecules. After 163 °C, a gradual weight loss until 800 °C is assigned to the loss of six dehydration protons, four imidazolium cations, three succinic acid ligands and the sublimation of metal oxides. For compound **2**, the first weight loss of 2.00% (calc. 1.96%) from 25 to 163 °C is attributed to the remove of 3.5 lattice water molecules, and the second weight loss 45.84% between 163–800 °C corresponds to the release of two dehydration protons, eight imidazolium cations, three suberic acid ligands and the sublimation of metal oxides. For compound **3**, the first weight loss 4.56% (calc. 4.64%) from 25 to 197 °C arises from the release of sixteen lattice water molecules, and after 197 °C, a gradual weight loss until 800 °C corresponds to the loss of four dehydration protons, sixteen guanidine hydrochloride molecules, four $btcH_3$ ligands and the sublimation of metal oxides.

Conclusions

In summary, we took advantage of two aliphatic carboxylic acids and an aromatic carboxylic acid to modify telluromolybdates and obtained two dimers and a tetramer, indicating the inherent nature of carboxylic acid ligands directing and controlling the structures of the inorganic–organic hybrids, simultaneously highlighting the structure-directing role of carboxylate linkers in the polyoxoanions self-assembly processes. Broadly speaking, the formation of carboxyl-oriented deliberate architectures shows that a great deal of structural design is possible in the covalently functionalized POMs assemblies. Furthermore, we explored their intriguing thermosensitivity as well as photochromic properties and found they had different allochroic behaviors. A further study was carried out and the mechanism was explained. The hybrids may have applications in the fields of thermosensitive and photosensitive materials. Next, we will utilize novel carboxylic acid ligands and other heteroatoms to explore this field of inorganic–organic POM hybrids ulteriorly.

Acknowledgements

The authors thank the National Natural Science Foundation of China, the Foundation of Education Department of Henan Province and Natural Science Foundation of Henan Province for financial support.

Notes and references

1 (*a*) A. Dolbecq, E. Dumas, C. R. Mayer and P. Mialane, *Chem. Rev.*, 2010, **110**, 6009; (*b*) A. Proust, R. Thouvenot and P. Gouzerh, *Chem. Commun.*, 2008, 1837; (*c*) P. Gouzerh and A. Proust, *Chem. Rev.*, 1998, **98**, 77; (*d*) Y. Jia, H. Q. Tan, Z. M. Zhang and E. B. Wang, *J. Mater. Chem. C*, 2013, **1**, 3681; (*e*) A. Saad, O. Oms, J. Marrot, A. Dolbecq, K. Hakouk, H. E. Bekkachi, S. Jobic, P. Deniard, R. Dessapt, D. Garrot, K. Boukheddaden, R. J. Liu, G. J. Zhang, B. Keita and P. Mialane, *J. Mater. Chem. C*, 2014, **2**, 4748; (*f*) L. Yue, H. Ai, Y. Yang, W. J. Lu and L. X. Wu, *Chem. Commun.*, 2013, **49**, 9770; (*g*) Y. F. Song, N. McMillan, D. L. Long, J. Thiel, Y. L. Ding, H. S. Chen, N. Gadegaard and L. Cronin, *Chem. – Eur. J.*, 2008, **14**, 2349.

2 (*a*) U. Kortz, M. G. Savelieff, F. Y. AbouGhali, L. M. Khalil, S. A. Maalouf and D. I. Sinno, *Angew. Chem., Int. Ed.*, 2002, **41**, 4070; (*b*) U. Kortz, J. Vaissermann, R. Thouvenot and P. Gouzerh, *Inorg. Chem.*, 2003, **42**, 1135; (*c*) W. Ouellette, M. H. Yu, C. J. O'Connor and J. Zubieta, *Inorg. Chem.*, 2006, **45**, 3224; (*d*) C. R. Mayer, V. Cabuil, T. Lalot and R. Thouvenot, *Angew. Chem., Int. Ed.*, 1999, **38**, 3672; (*e*) B. Zhang, L. Yue, Y. Wang, Y. Yang and L. X. Wu, *Chem. Commun.*, 2014, **50**, 10823; (*f*) Y. F. Song and L. Cronin, *Angew. Chem., Int. Ed.*, 2008, **47**, 4635.

3 (*a*) R. Dessapt, M. Collet, V. Coué, M. Bujoli-Doeuff, S. Jobic, C. Lee and M.-H. Whangbo, *Inorg. Chem.*, 2009, **48**, 574; (*b*) K. Hakouk, O. Oms, A. Dolbecq, H. El Moll, J. Marrot, M. Evain, F. Molton, C. Duboc, P. Deniard, S. Jobic, P. Mialane and R. Dessapt, *Inorg. Chem.*, 2013, **52**, 555; (*c*) J. D. Compain, P. Deniard, R. Dessapt, A. Dolbecq, O. Oms, F. Secheresse, J. Marrot and P. Mialane, *Chem. Commun.*, 2010, **46**, 7733; (*d*) R. Dessapt, M. Gabard, M. Bujoli-Doeuff, P. Deniard and S. Jobic, *Inorg. Chem.*, 2011, **50**, 8790.

4 M. Gaudon, C. Carbonera, A. E. Thiry, A. Demourgues, P. Deniard, C. Payen, J.-F. Létard and S. Jobic, *Inorg. Chem.*, 2007, **46**, 10200.

5 B. Salignac, S. Riedel, A. Dolbecq, F. Sécheresse and E. Cadot, *J. Am. Chem. Soc.*, 2000, **122**, 10381.

6 (*a*) Z. H. Zhou, S. Y. Hou, Z. X. Cao, H. L. Wan and S.-W. Ng, *J. Inorg. Biochem.*, 2004, **98**, 1037; (*b*) Z. H. Zhou, S. Y. Hou, Z. X. Cao, K. R. Tsai and Y. L. Chow, *Inorg. Chem.*, 2006, **45**, 8447; (*c*) B. Modec, J. V. Brenčič, D. Dolenc and J. Zubieta, *Dalton Trans.*, 2002, 4582; (*d*) B. Modec, J. V. Brenčič, E. M. Burkholder and J. Zubieta, *Dalton Trans.*, 2003, 4618.

7 C. Hofmann, J. H. Thurston, K. B. Hartman, L. B. Alemany and K. H. Whitmire, *Inorg. Chim. Acta*, 2009, **362**, 1665.

8 (*a*) G. Liu, S. W. Zhang and Y. Q. Tang, *J. Chem. Soc., Dalton Trans.*, 2002, 2036; (*b*) G. G. Gao, L. Xu, X. S. Qu, H. Liu and Y. Y. Yang, *Inorg. Chem.*, 2008, **47**, 3402.

9 G. Liu, Q. Li and S. W. Zhang, *Inorg. Chem. Commun.*, 2002, **5**, 427.

10 W. Yang, C. Lu, X. Lin and H. Zhuang, *Inorg. Chem.*, 2002, **41**, 452.

11 (*a*) J.-F. Lemonnier, S. Floquet, J. Marrot, E. Terazzi, C. Piguet, P. Lesot, A. Pinto and E. Cadot, *Chem. – Eur. J.*, 2007, **13**, 3548; (*b*) J.-F. Lemonnier, S. Floquet, A. Kachmar, M.-M. Rohmer, M. Bénard, J. Marrot, E. Terazzi, C. Piguet and E. Cadot, *Dalton Trans.*, 2007, 3043; (*c*) J.-F. Lemonnier, A. Kachmar, S. Floquet, J. Marrot, M.-M. Rohmer, M. Bénard and E. Cadot, *Dalton Trans.*, 2008, 4565; (*d*) E. Cadot and

F. Sécheresse, *Chem. Commun.*, 2002, 2189; (*e*) A. Hijazi, J. C. Kemmegne-Mbouguen, S. Floquet, J. Marrot, J. Fize, V. Artero and E. Cadot, *Dalton Trans.*, 2013, **42**, 4848; (*f*) A. Dolbecq, E. Cadot and F. Sécheresse, *C. R. Acad. Sci., Ser. IIC: Chim.*, 2000, **3**, 193; (*g*) S. Floquet, J. Marrot and E. Cadot, *C. R. Chim.*, 2005, **8**, 1067.

12 (*a*) D. H. Yang, S. Z. Li, P. T. Ma, J. P. Wang and J. Y. Niu, *Inorg. Chem.*, 2013, **52**, 8987; (*b*) D. H. Yang, S. Z. Li, P. T. Ma, J. P. Wang and J. Y. Niu, *Inorg. Chem.*, 2013, **52**, 14034; (*c*) D. H. Yang, Y. F. Liang, P. T. Ma, S. Z. Li, J. P. Wang and J. Y. Niu, *Inorg. Chem.*, 2014, **53**, 3048; (*d*) D. H. Yang, Y. F. Liang, P. T. Ma, S. Z. Li, J. P. Wang and J. Y. Niu, *CrystEngComm*, 2014, **16**, 8041.

13 G. G. Gao, L. Xu, X. S. Qu, H. Liu and Y. Y. Yang, *Inorg. Chem.*, 2008, **47**, 3402.

14 V. Balraj and K. Vidyasagar, *Inorg. Chem.*, 1998, **37**, 4764.

15 (*a*) V. Balraj and K. Vidyasagar, *Inorg. Chem.*, 1999, **38**, 3458; (*b*) B. Modec, D. Dolenc and M. Kasunič, *Inorg. Chem.*, 2008, **47**, 3625.

16 V. Coué, R. Dessapt, M. Bujoli-Doeuff, M. Evain and S. Jobic, *Inorg. Chem.*, 2007, **46**, 2824.

17 H. Zhang, Y. L. Duan, Y. Lan, E. B. Wang and C. W. Hu, *Inorg. Chem.*, 2003, **42**, 8053.

18 C. Baffert, J. F. Boas, A. M. Bond, P. Kçgerler, D. L. Long, J. R. Pilbrow and L. Cronin, *Chem. – Eur. J.*, 2006, **12**, 8472.

19 G. G. Gao, L. Xu, X. S. Qu, H. Liu and Y. Y. Yang, *Inorg. Chem.*, 2008, **47**, 3402.

20 T. Yamase, *Chem. Rev.*, 1998, **98**, 307.

21 (*a*) H. E. Moll, A. Dolbecq, I. M. Mbomekalle, J. Marrot, P. Deniard, R. Dessapt and P. Mialane, *Inorg. Chem.*, 2012, **51**, 2291; (*b*) L. Yang, Z. Zhou, P. T. Ma, J. P. Wang and J. Y. Niu, *Cryst. Growth Des.*, 2013, **13**, 2540.